Composites Science and Technology 68 (2008) 2141–2148

Contents lists available at ScienceDirect

Composites Science and Technology

journal homepage: www.elsevier.com/locate/compscitech

# Effect of microstructural evolution on mechanical properties of friction stir welded AA2009/SiCp composite

A.H. Feng, B.L. Xiao, Z.Y. Ma *

*Shenyang National Laboratory for Materials Science, Institute of Metal Research, Chinese Academy of Sciences, 72 Wenhua Road, Shenyang 110016, China*

ARTICLE INFO

*Article history:*
Received 27 July 2007
Received in revised form 25 February 2008
Accepted 18 March 2008
Available online 25 March 2008

*Keywords:*
Friction stir welding
A. Metal–matrix composites (MMCs)
B. Mechanical properties
E. Powder processing
B. Fracture

ABSTRACT

Extruded AA2009/15%/SiCp composite was friction stir welded (FSW) and subjected to subsequent post-weld T4-treatment. FSW resulted in significant grain refinement, breaking and uniform distribution of SiC particles, dissolution of coarse needle-shaped precipitates and re-precipitation in the nugget zone, thereby increasing the hardness and longitudinal and transverse strengths of the as-FSW composite joint remarkably. Post-weld T4-treatment resulted in limited grain growth and improved weld strength. Under the T4 condition, the longitudinal and transverse tensile strengths of the weld reached 82% and 95% of the base metal, respectively. The low joining efficiency under the T4 condition was associated with the formation of the $Cu_2FeAl_7$ phase.



## 1. Introduction

Fabrication of complicated components of metal–matrix composites (MMCs) depends on effective joining methods such as solid state and fusion processes, which are still specific material and process dependent. It is hard to achieve defect-free welds by using conventional fusion welding techniques [1]. The drawbacks associated with the fusion welding include: (a) the incomplete mixing of the parent and filler materials, (b) the presence of porosity as large as 100 μm in the fusion zone, (c) the excess eutectic formation, and (d) the formation of undesirable deleterious phases such as $Al_4C_3$. Therefore, a solid state welding technique is highly desirable for joining MMCs.

Friction stir welding (FSW) is a relatively new solid state joining technique developed for joining aluminum alloys [2,3]. Since the invention of FSW at The Welding Institute (TWI) of the UK in 1991 [3], the rapid development and successful commercial application of the FSW technique with aluminum alloys have encouraged its application to other metallic materials (Mg, Cu, Ti, and steel) and dissimilar alloys/metals [2]. Recently, several studies were conducted to evaluate the feasibility of FSW of aluminum–matrix composites [4–10]. It was discovered that high-quality welds without visible defects could be generated by FSW. The homogeneous distribution of reinforcements and improved joint efficiencies were reported [7,8,11].

However, FSW has specific limitations for the aluminum–matrix composites (AMCs) due to their low ductility and high wear resistance. Therefore, the FSW parameter range for producing sound welds in the AMCs was obviously narrower than that in the unreinforced alloys [8] and severe tool wear occurred during the FSW due to the presence of hard ceramic reinforcements [5]. Considering the fact that the AMCs under as-extruded or rolled conditions have lower hardness/strength and higher plasticity, it is expected that sound welds will be easily achieved under a soft condition with reduced tool wear and welding load. After FSW, the mechanical properties of the welds can be enhanced by the post-weld heat treatment (PWHT). For some aluminum alloys, when the FSW joints were subjected to a PWHT at high-temperature, abnormal grain growth (AGG) occurred in the nugget zone (NZ) because the fine-grained structure was inherently instable, which was explained by the theory of cellular microstructure proposed by Humphreys [12]. However, the presence of dispersoid particles will inhibit grain boundary mobility if they do not dissolve during solution treatment [13]. Because of this, when the FSW composite weld is subjected to the high-temperature PWHT the AGG will not take place due to the presence of numerous SiC particles.

In a previous paper [14], the present authors reported successful welding of 8 mm thick as-extruded AA2009/SiCp composite plates. Furthermore, the formation of the $Cu_2FeAl_7$ phase was identified at or near the SiC particle interfaces in the FSW composite [15]. In this study, as-FSW and PWHT AA2009/SiCp composite welds were subjected to detailed microstructural examination and property evaluation. The purpose is (a) to study microstructure

* Corresponding author. Tel./fax: +86 24 83978908.
*E-mail address:* zyma@imr.ac.cn (Z.Y. Ma).

0266-3538/$ - see front matter © 2008 Elsevier Ltd. All rights reserved.
doi:10.1016/j.compscitech.2008.03.010

evolution during FSW, (b) to evaluate the effect of post-weld T4 on the microstructure and properties of the welds, and (c) examine the effect of the $Cu_2FeAl_7$ phase on the mechanical properties of the welds.

## 2. Experimental

AA2009/15%/SiCp composite, produced by powder metallurgy and subsequent extrusion, was used in this study. The chemical composition of the AA2009 alloy was 4.26Cu–1.61Mg–0.01Si–0.009Fe (wt.%). 8 mm thick plates were cut from the extruded bars and friction stir welded along the extrusion direction at a tool rotation rate of 600 rpm and a traverse speed of 50 mm/min. A steel tool with a shoulder 24 mm in diameter and a cylindrical threaded pin 8 mm in diameter was used. Following the FSW, samples were kept at room temperature for one month to age naturally. In order to study the effect of the PWHT, part of the FSW samples were T4-treated (solutionized at 502 °C for 1 h, water quenched, and then aged at room temperature for one month).

The microstructure was examined using optical microscopy (OM), scanning electron microscopy (SEM, Hitachi S-3400 N), and transmission electron microscopy (TEM). Quantitative X-ray analysis was conducted on a D/max 2500PC diffractometer at 50 kV and 250 mA, using Cu-K$\alpha$ radiation ($\lambda$ = 1.5418 Å) and subsequent JADE 5.0 software. The iron concentration in the as-extruded composite was determined by using a PW4400 X-ray fluorescence spectrometer with an irradiation diameter of at least 25 mm.

The hardness profiles were produced along the mid-thickness on the cross section of the welds by using a Vickers hardness tester at a 1 kg load. Transverse and longitudinal tensile specimens were machined from the FSW samples perpendicular and parallel to the welding direction, respectively. The longitudinal tensile specimens contain only the NZ. Tensile tests were conducted at room temperature at an initial strain rate of $1 \times 10^{-3}\ s^{-1}$. The fracture surfaces of tensile specimens were examined using SEM.

## 3. Results

As in FSW aluminum alloys, the FSW composite joint consisted of three zones: the NZ, the thermomechanically affected zone (TMAZ), and the heat affected zone (HAZ) (Fig. 1a). The NZ exhibited an elliptical shape and onion rings were distinctly visible. After T4-treatment, the macrostructure of the weld did not change fundamentally and no AGG was detected (Fig. 1b).

Fig. 2 shows the microstructure of the AA2009/SiCp composites under various conditions. In the base metal (BM), the particle clusters and particle-free regions were evidently visible and the microstructure was characterized by nonuniformly distributed SiC particles and coarse grains (Fig. 2a). After FSW, the distribution of SiC particles in the NZ was significantly improved and the microstructure was characterized by homogenously distributed SiC particles and fine equiaxed recrystallized grains of ~5 μm (Fig. 2c). Compared to the sharp SiC particles in the as-extruded composite (Fig. 2b), the edges and corners of the SiC particles in the NZ were obviously blunted and micro-cracks were detected in some large SiC particles (Fig. 2d). Furthermore, the size and aspect ratio of the SiC particles were obviously decreased after FSW. The average size of the SiC particles decreased from ~5.4 μm in the as-extruded composites to ~4.2 μm in the NZ of the as-FSW composite. The post-weld T4-treatment resulted in grain growth in the NZ with the grain size increasing to ~8 μm (Fig. 2e). However, no AGG was detected. Moreover, after T4-treatment, the number of fine particles in the NZ tended to decrease (Fig. 2d and f). The magnified view of the onion rings (as shown in Fig. 1) indicated that the onion rings consisted of fine particle-rich bands (Fig. 3). The fine particles in the particle-rich bands were identified to be Al–Cu–Fe–Mg and Al–Cu–Fe phases by EDS (Table 1).

The X-ray diffraction (XRD) pattern of the as-extruded 2009Al alloy revealed the presence of $Al_2CuMg$ and $CuAl_2$ phases, which are two types of precipitates in Al–Cu–Mg alloys. For the as-extruded composite, in addition to Al, $Al_2CuMg$, $CuAl_2$, and $\alpha$-SiC peaks, a diffraction peak corresponding to the (2 1 4) plane of $Cu_2FeAl_7$ was detected (Fig. 4a). In the NZ of the as-FSW composite, besides Al, $CuAl_2$, and $\alpha$-SiC peaks, $Cu_2FeAl_7$ diffraction lines were distinctly visible, indicating the formation of $Cu_2FeAl_7$ phase (Fig. 4b). Compared with the as-extruded composite, the diffraction peaks of $CuAl_2$ decreased in the NZ of the as-FSW composite, indicating the partial dissolution of $CuAl_2$ phase. On the other hand, the diffraction peaks of the HAZ of the as-FSW composite were quite similar to those of the as-extruded composite, i.e., besides Al, $Al_2CuMg$, $CuAl_2$, and $\alpha$-SiC peaks, an additional diffraction peak corresponding to the (2 1 4) plane of the $Cu_2FeAl_7$ was found (Fig. 4c). The intensity of the $CuAl_2$ diffraction peaks in the NZ of the FSW composite was remarkably reduced after T4-treatment and the $Al_2CuMg$ diffraction peak appeared (Fig. 4d).

In the as-extruded composite, the coarse needle-shaped precipitates were evidently visible, which were identified to be $\theta$ $CuAl_2$ (Fig. 5a). After FSW, the coarse needle-shaped $\theta$ precipitates disappeared in the NZ. A number of fine precipitates were detected within the grains and they were identified to be $\theta''$ $CuAl_2$ phase by microdiffraction patterns (Fig. 5b). The $\theta''$ phase is one of the main hardening precipitates in the Al–Cu–Mg alloys. After post-weld T4-treatment, the number of $\theta''$ phase in the NZ increased (Fig. 5c). Meanwhile, the fine needle-shaped $S'$ ($Al_2CuMg$) precipitates were also observed (Fig. 5d).

Fig. 6 shows the hardness profiles along the mid-thickness on the cross section of the FSW composite. Under the as-FSW condition, the maximum hardness of ~155 Hv was observed in a zone ~10 mm wide around the weld centerline. This hardness plateau corresponds to the width of the NZ. Beyond the hardness plateau, the hardness decreased gradually with increasing distance from the NZ. On the advancing side, the hardness decreased to the level of the BM at ~19 mm from the weld centerline and there appeared an unobvious minimum hardness zone at 24 mm from the weld centerline. On the retreating side, the hardness reached the level of the BM at ~17 mm from the weld centerline and there was no noticeable minimum hardness zone. After the T4-treatment, the hardness of the BM, TMAZ, and HAZ increased significantly. However, the hardness of the NZ exhibited only a slight increase and was somewhat lower than that of other regions.

Tensile properties of the FSW composite joints are shown in Fig. 7. The tensile and yield strengths of the as-FSW composite along both the longitudinal and transverse directions were superior to those of the as-extruded composite (Fig. 7a and b). After

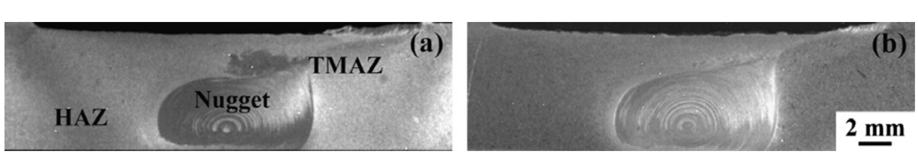


**Fig. 1.** Macrographs showing cross section of FSW AA2009/SiCp composite joint (etched by mixed acids): (a) as-FSW condition and (b) T4-treatment condition.

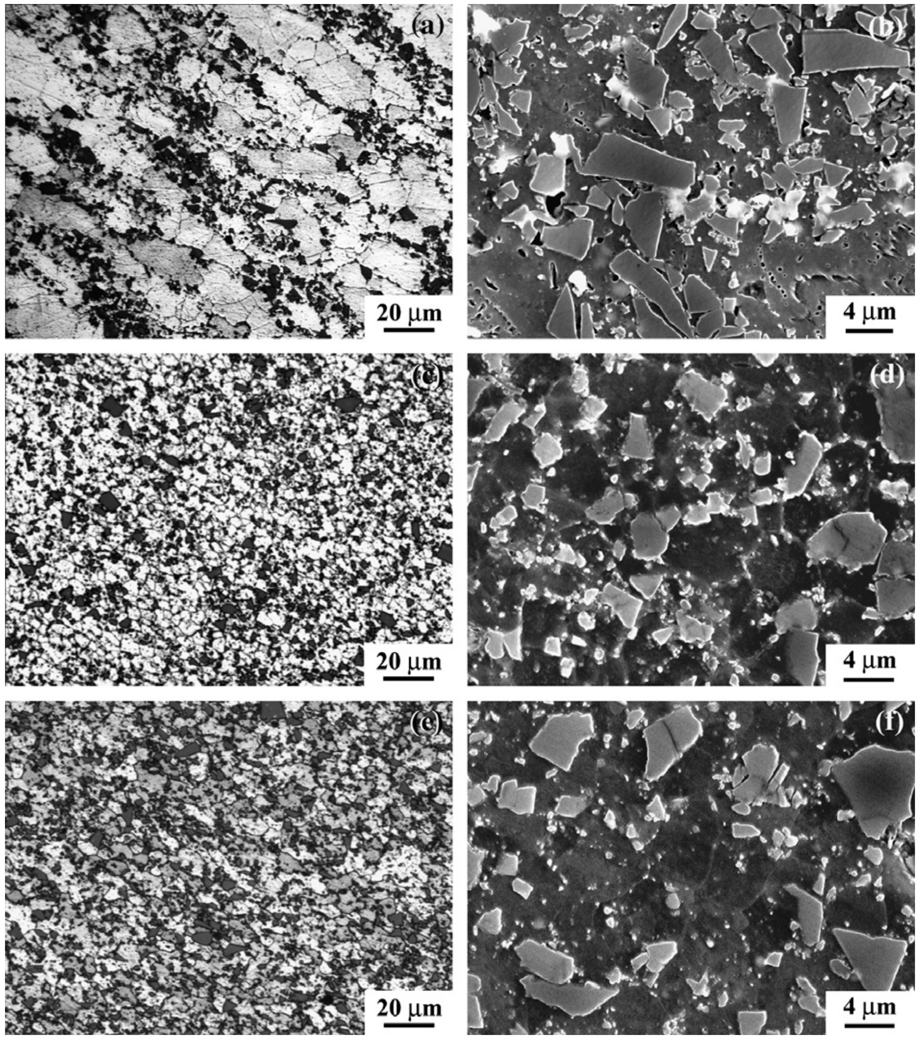


**Fig. 2.** Microstructure of AA2009/SiCp composites: (a) and (b) base metal, (c) and (d) nugget zone under as-FSW condition, (e) and (f) nugget zone under T4-treatment condition; (a), (c), (e) OM and (b), (d), (f) SEM.

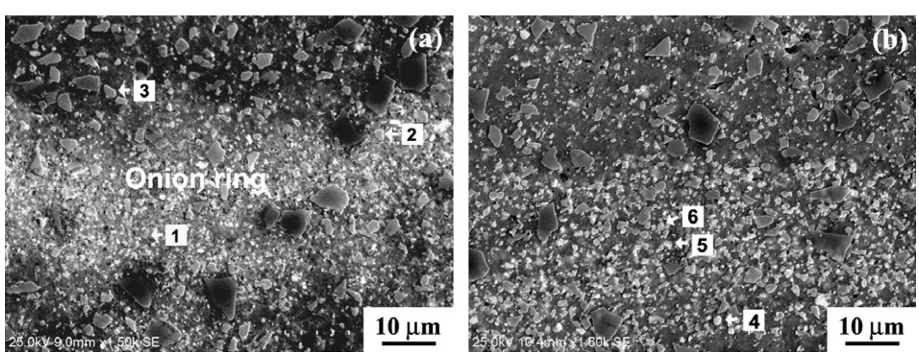


**Fig. 3.** SEM micrographs showing fine particle-rich bands in onion rings in nugget zone of FSW composites: (a) as-FSW condition, (b) T4-treatment condition.

T4-treatment, the strength of both the BM and the FSW sample increased. However, under the T4-treated condition, the strength of the FSW composite was lower than that of the BM in both transverse and longitudinal directions (Fig. 7c and d).

Fig. 8 shows the tensile fracture surfaces of the longitudinal specimens for the T4-treated extruded and FSW samples. The fracture surface of the T4-treated extruded composites was characterized by micro-dimples and tearing ridges, and particle pullout and cracking were seldom observed (Fig. 8a). However, for the T4-treated FSW sample, there were more SiC particle pullout and cracking (Fig. 8b). SEM backscattered electron image indicated that the SiC particle pullout was often associated with white small particles, as shown by white arrow in Fig. 8c. EDS analyses revealed that the white particle near the SiC interface contained high ratios of Cu and Fe (Cu: 24.96 wt.%, Fe: 12.32 wt.%), indicating that the white particles were $Cu_2FeAl_7$ phase.

**Table 1**
The results of EDS analysis of Fig. 3 (wt.%)

| Location | Al | Cu | Mg | Fe |
|---|---|---|---|---|
| 1 | 77.65 | 9.44 | 1.23 | 11.68 |
| 2 | 88.80 | 8.51 | 1.20 | 1.49 |
| 3 | 91.86 | 6.78 | 1.35 | – |
| 4 | 79.57 | 16.02 | 1.20 | 3.21 |
| 5 | 69.07 | 23.81 | – | 7.12 |
| 6 | 68.10 | 25.30 | 1.30 | 5.30 |

## 4. Discussion

### 4.1. Microstructural evolution

Onion rings with the swirl patterns in a plane 90° to the rotation plane of the tool pin (the typical structure found on the cross sections of FSW aluminum alloys) were evidently visible in the NZ of the FSW composite (Fig. 1). The formation of the onion rings has been explained by the geometrical effect [16], the variations in grain size [17], and particle-rich bands [17,18]. A recent study on FSW 2024Al-T351 alloy by Sutton et al. [18] showed that a segregated, banded microstructure consisting of alternating hard particle-rich and hard particle-poor regions developed in the NZ. Sutton et al. suggested that the particle segregation resulted from the entrainment of the particles with appropriate size in the region corresponding to high strain rate gradient [18]. In a very recent study, Uzun [9] found that the banded microstructure in the NZ of FSW SiCp/2124Al consisted of segregated fine SiC particles within these bands and exhibited the alternating regions of high and low fine SiC particle density. The present SEM examinations showed that the onion rings in the NZ of the FSW composite consisted of fine particle-rich bands, and the SiC particles did not segregate in the onion rings (Fig. 3). These fine particles were identified to be Al–Cu–Fe–Mg and Al–Cu–Fe phases (Table 1). Clearly, the present observation of the formation of the onion rings is different from that of Uzun [9]. The possible reason is that the high strain rate gradient was not sufficient to drive the larger SiC particles to segregate to the high density bands of particles.

In the as-extruded composite, particle clusters were obviously visible due to insufficient plastic strain (Fig. 2a). After FSW, the SiC particle distribution was significantly improved due to intense plastic deformation and material mixing (Fig. 2c). Furthermore, the rotating pin produced a breaking effect on the SiC particles, resulting in the knocking off of corners and sharp edges from the large particles and cracking of some large particles, therefore, the size and aspect ratio of the SiC particles decreased obviously (Fig. 2d and f). Similar observations have been made in FSW AMCs by other investigators [5]. Based on the average size of SiC particles, the mean interparticle distance in the FSW composite was estimated to be ~6.4 μm in the case of the mean spatial distribution of SiC particle in the matrix. Only when the particle size is less than 0.1 μm and the interparticle spacing is less than 1.5 μm can recrystallization be inhibited, because the dislocation cell structure in the deformed metal becomes anchored and stabilized by the particles [19]. Therefore, there is enough space for the matrix of the composite to recrystallize in the NZ.

The fine and equiaxed grains of ~5 μm in the NZ of the as-FSW composite were much smaller than those in the BM (Fig. 2a and b). This indicated that dynamic recrystallization (DRX) took place in the NZ of the FSW composite during the FSW process. Like any recrystallization process, DRX proceeds by nucleation and nucleus growth. However, there is still a lack of understanding of the underlying physical processes that control DRX, especially in the FSW process. Proposed recrystallization mechanisms during FSW include: the continuous dynamic recrystallization (CDRX) [20], the geometric dynamic recrystallization (GDRX) [21], and the discontinuous dynamic recrystallization (DDRX) [21].

DRX has long been considered to be restricted to low stacking fault energy (SFE) metals, such as copper, γ-iron, and austenitic steels [22]. In high SFE metals (aluminum, α-iron, ferritic steels), dynamic recovery is assumed to be the only operating mechanism.

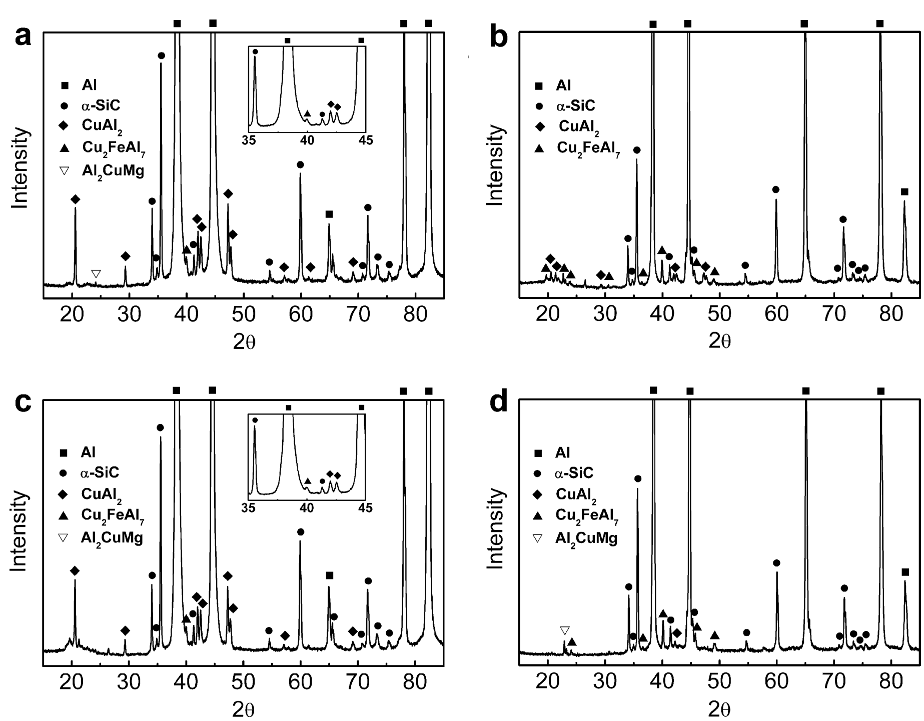


**Fig. 4.** X-ray diffraction patterns: (a) as-extruded composite, (b) nugget zone in as-FSW composite, (c) HAZ in as-FSW composite, (d) nugget zone in T4-treated FSW composite.

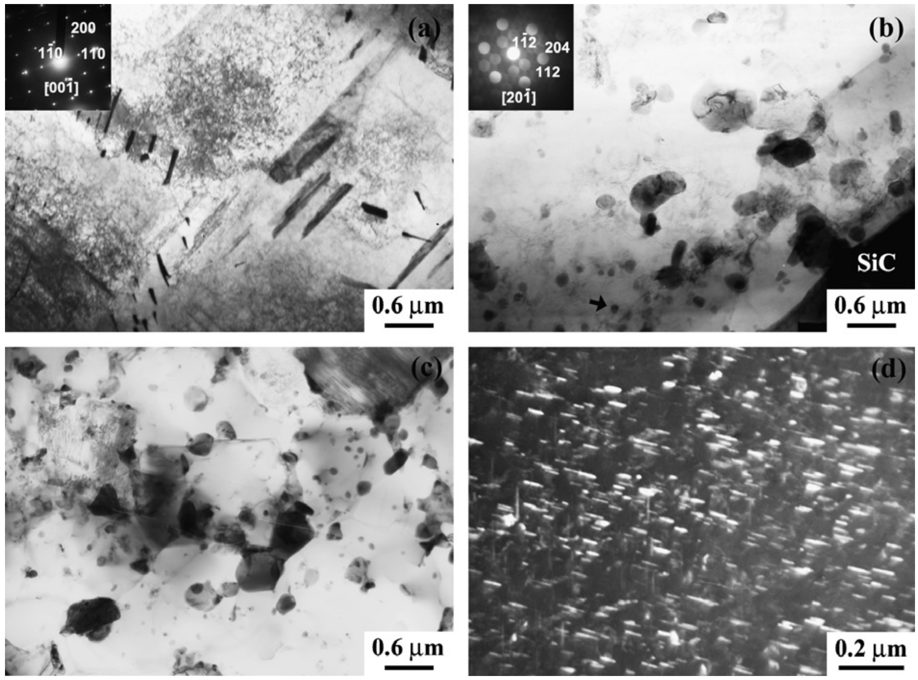


**Fig. 5.** TEM micrographs showing distribution of precipitates in (a) as-extruded composite, (b) nugget zone in as-FSW composite, (c) and (d) nugget zone in T4-treated FSW composite.

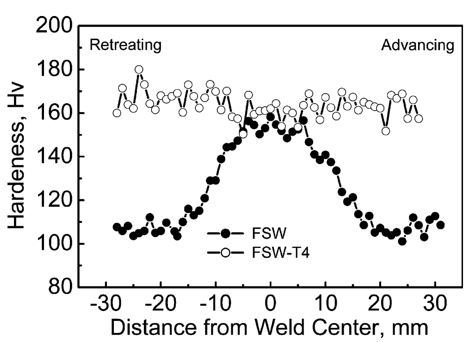


**Fig. 6.** Microhardness profiles for AA2009/SiCp composite weld.

However, recent research indicates that DRX could occur in the aluminum-based alloys during hot deformation such as hot torsion and extrusion [23–25]. It was reported that deformation efficiency for DRX depends on alloy composition, crystal structure, and deformation history, as well as the SFE of the alloy [24]. The relationship between the recrystallized grain size and the Zener–Hollomon parameter has been well analyzed [24]. SiC particles had a large effect on the recrystallization kinetics [25]. The DRX nucleated in regions of very high dislocation density between the reinforcements [23]. Inem [25] found that the SiC particles provided more nucleation sites for the new recrystallized grains by increasing local strain in the matrix and causing lattice misorientation. The particles play an important role in controlling the recrystallized grain size by particle stimulated nucleation. If each particle produces one recrystallized grain, then the resultant grain size $D$ will be directly related to the volume fraction $Fv$ and the diameter of particles $d$ by [26]:

$$D \approx dFv^{-1/3}. \tag{1}$$

According to Eq. (1), the predicted recrystallized grain size ($\sim$8 μm) is larger than the actual average grain size ($\sim$5 μm) in the NZ of the FSW composite, indicating that there were other factors influencing the recrystallization kinetics such as the precipitation and the particle dispersion level. Furthermore, secondary phase particles with diameters larger than 1.0 μm may stimulate the nucleation of recrystallized grains in the deformation zone adjacent to the particles because of more stored energy in the zones around the particles than far from the particles [27]. Therefore, the particles that can stimulate the recrystallization nucleation included not only the SiC particles but also other particles with a diameter larger than 1.0 μm, which explains the discrepancy between the predicted recrystallized grain size and the actual average grain size. After T4-treatment, the limited grain growth is attributed to the effective pinning of the SiC particles, which was also observed in the SiCp/ZC71 composite [25].

FSW can be considered a hot-working process in which severe plastic deformation is imparted to the workpiece through the rotating pin and shoulder. The maximum temperatures can exceed $0.8T_m$ in aluminum alloys (where $T_m$ is the melting temperature of aluminum expressed in K), which is enough to induce the partial dissolution of the hardening precipitates. Transient high-temperature and severe plastic deformation with a strain rate of $10^0$–$10^2\ s^{-1}$ and a strain of up to $\sim$40 in the NZ [28,29] resulted in breaking and partial dissolution of the coarse precipitates in the as-extruded composite into the aluminum–matrix in the NZ (Fig. 5a and b). During natural aging after FSW, re-precipitation of the dissolved precipitates occurred in the NZ (Fig. 5b). According to the TEM microdiffraction patterns, the main hardening precipitate was the $\theta''$ phase under as-FSW condition. After post-weld T4-treatment, all the precipitates dissolved into the aluminum–matrix and then precipitated as the fine $\theta''$ phase and needle-shaped $S'$ phase (Fig. 5c and d).

### 4.2. Quantitatively analysis of the $Cu_2FeAl_7$ phase

In a recent study, the formation of the $Cu_2FeAl_7$ phase was identified at or near the SiC particle interfaces in the FSW AA2009/SiCp composite [15]. Here, a quantitative analysis by XRD was carried

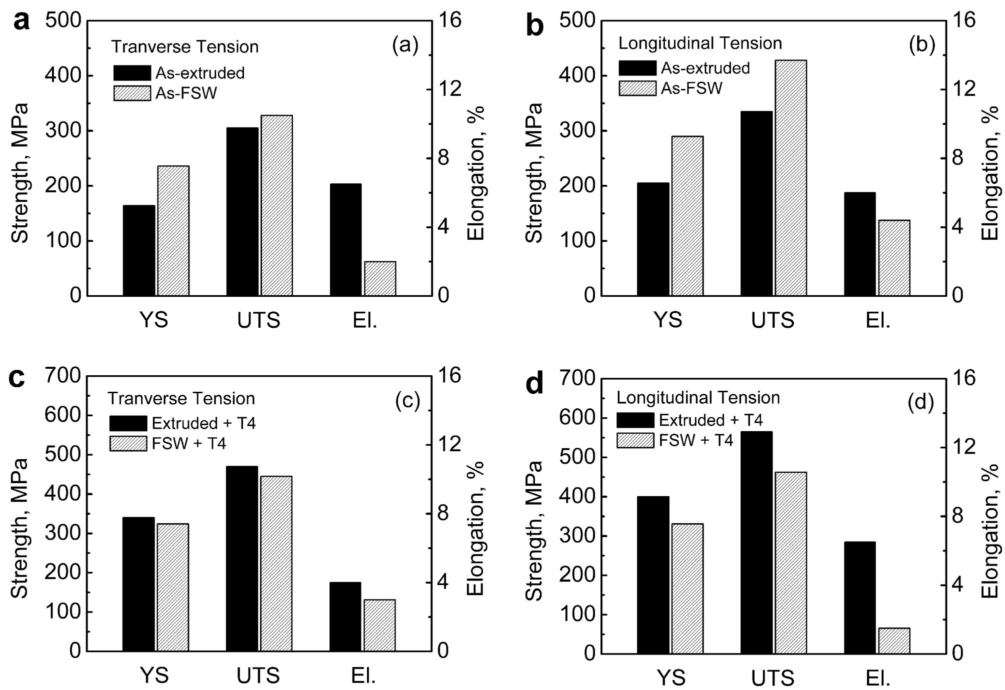


**Fig. 7.** Tensile properties of AA2009/SiCp composites: (a) and (b) as-extruded or as-FSW, (c) and (d) T4-treated; (a) and (c) transverse tension, (b) and (d) longitudinal tension.

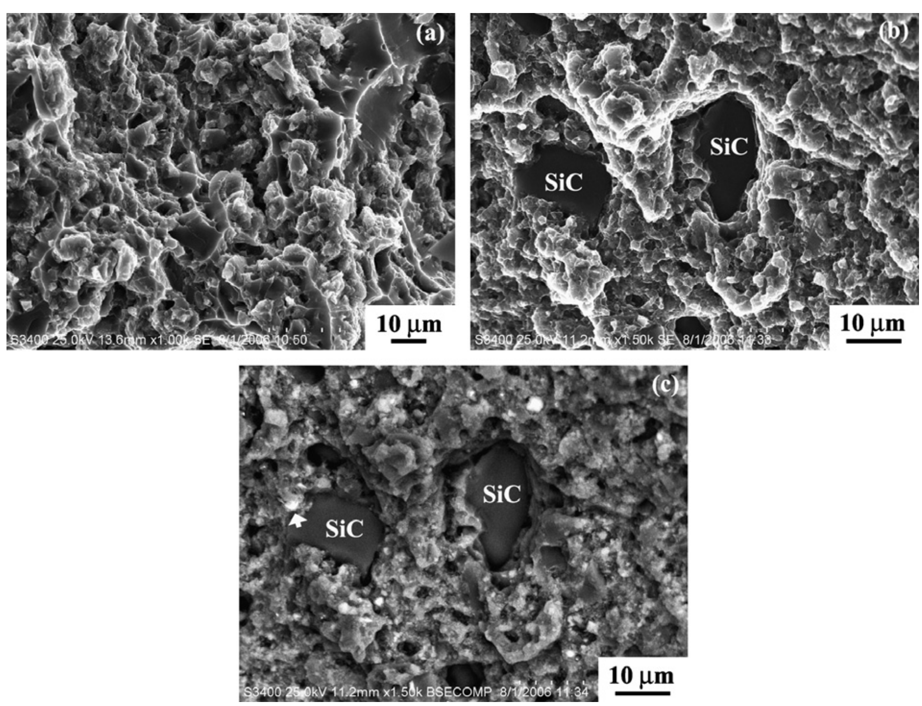


**Fig. 8.** SEM images showing fracture surfaces of longitudinal tensile specimens of T4-treated composite: (a) base metal, secondary electron image (SEI), (b) FSW sample, SEI, (c) FSW sample, backscattered electron image (BEI).

out to estimate the content of the $Cu_2FeAl_7$ phase in the FSW composites, based on the following equation [30]:

$$\frac{I_{ij}}{I_{ks}} = K' \frac{x_j}{x_s}, \quad (2)$$

where $I_{ij}$ is the intensity of diffraction line $i$ of phase $j$ in a material, $I_{ks}$ is the intensity of diffraction line $k$ of phase $s$, $x_j$ is the weight fraction of phase $j$, $x_s$ is the weight fraction of phase $s$, and $K'$ is a constant. In this study, the diffraction line of (108) of SiC and the diffraction line of (214) of $Cu_2FeAl_7$ were used for the quantitative calculation.

Suppose that the weight fraction of the SiC particle is constant in both as-extruded and as-FSW composites and the ratio of weight fraction/peak intensity is constant for both SiC and $Cu_2FeAl_7$ under various conditions, then the weight fraction of the $Cu_2FeAl_7$ phase can be calculated by using Eq. (2). The concentration of iron in as-extruded composite was determined to be 0.072 wt.% using an X-ray fluorescence spectrometer. We assume that all the iron was transformed to the $Cu_2FeAl_7$ phase, then the concentration of iron under various conditions is obtained based on Eq. (2).

In the AA2009 alloy, no $Cu_2FeAl_7$ or other compounds containing Fe was detected in the XRD pattern due to a very low Fe concentration of 0.009 wt.%. In the as-extruded AA2009/SiCp composite, the Fe concentration of 0.072 wt.% increased by 7.8 times compared to that in the unreinforced AA2009 alloy. The higher Fe concentration of 0.072 wt.% was caused by the mixing process of SiC–Al powder. During the fabrication of the composite, SiC and aluminum powders were mixed in a steel vessel with steel balls. In this case, Fe contamination of mixed powders was inevitable. In the NZ of the as-FSW and T4-treated composites, the Fe concentration was calculated to be as high as 0.167 and 0.222 wt.%, respectively, according to Eq. (2). The significantly increased Fe concentration was attributed to the tool wear due to the presence of hard SiC particles. After a FSW of the composite 400 mm in length, it was found that the diameter of the pin was reduced from 8 mm to ~7.7 mm. It is expected that there was higher Fe concentration around the SiC particles because the tool wear was caused by hard and sharp SiC particles. Such a higher Fe concentration justifies the formation of the $Cu_2FeAl_7$ phase according to the Al–Cu–Fe liquidus projection diagram [31]. In the HAZ of the FSW composite, the Fe concentration of 0.073 wt.%, as calculated by Eq. (2), did not increase compared to that in the as-extruded composite. This is consistent with the XRD results (Fig. 4a and c). It is not surprising considering the fact that the HAZ was not stirred by the tool pin during FSW.

### 4.3. Hardness and tensile properties

It was reported that the hardness profile of FSW heat-treatable aluminum alloys greatly depends on the precipitate distribution and only slightly on the grain and dislocation structures [32]. In the as-extruded composite, the coarse precipitates resulting from slow cooling after the extrusion did not exert an obvious strengthening effect on the aluminum–matrix. Therefore, the as-extruded composite exhibited a lower hardness of 105–110 Hv. As discussed above, FSW resulted in partial dissolution of the coarse precipitates and subsequent re-precipitation during natural aging after FSW (Fig. 5b). This resulted in a significant increase in the hardness of the NZ (Fig. 6). Furthermore, the refinement of both the SiC particles and the grains also contributed to the increase in the hardness of the NZ. After the T4-treatment, all the precipitates in various zones of the weld completely dissolved into the aluminum–matrix and then re-precipitated. In this case, the precipitation-strengthening effect was quite similar in various zones, therefore, similar hardness values were observed across the whole weld. However, it is noted in Fig. 6 that under the T4 condition, the hardness of the NZ was slightly lower than that of the TMAZ and HAZ. This might be associated with the formation of the $Cu_2FeAl_7$ phase, as will discussed later.

Fig. 7a and b shows that both tensile and yield strengths of the as-FSW composite weld were superior to those of the as-extruded composite along both longitudinal and transverse directions. The enhancement in the strength of the as-FSW composite weld was mainly attributed to the precipitation-strengthening resulting from the FSW thermal cycles as discussed above. Furthermore, the fine grain size and homogeneous distribution of the refined SiC particles also contributed to the improvement in the strength. However, under the T4 condition, both longitudinal and transverse strengths of the composite weld were lower than those of the BM. The T4-treatment only resulted in limited grain growth, therefore the grain microstructure was not a dominant factor affecting the strength of the weld. Based upon the microstructural observations, the lower strength and hardness of the composite weld compared to the BM under the T4 condition might be associated with the formation of $Cu_2FeAl_7$ at the SiCp/Al interfaces. First, the formation of $Cu_2FeAl_7$ reduced the interfacial bonding. The longitudinal tensile test showed that there were more pullouts of SiC particles on the fracture surfaces, which was usually associated with the $Cu_2FeAl_7$ particles at the SiC/Al interfaces (Fig. 8c). This indicates that the formation of $Cu_2FeAl_7$ phase indeed reduced the SiC/Al interfacial bonding, and the crack propagated primarily along the SiCp/Al interfaces. Second, the formation of $Cu_2FeAl_7$ phase reduced the amount of the precipitates due to the dilution of Cu. In this case, the precipitation-strengthening effect from the fine precipitates was reduced, thereby reducing the strength and hardness of the NZ of the T4-treated FSW composite (Figs. 6 and 7d). However, it should be pointed out that although the strength of the composite weld was lower than that of the BM under the T4 condition, the tensile strength of the welds along the longitudinal and transverse directions reached 82 and 95% of the BM, respectively. The joining efficiency is higher than that obtained by other investigators [4,6–8].

The present study indicates that it is feasible to join the AA2009/SiCp composite under a soft (extruded) condition via FSW and then strengthen the weld by a post-weld strengthening heat treatment that does not change the microstructure of the FSW composite joint significantly. Such a joining procedure is beneficial in achieving a defect-free weld and reducing tool wear and welding load. However, this study indicated that even slight tool wear resulted in a decrease in the strength of the composite weld due to the formation of the deleterious phase $Cu_2FeAl_7$. Therefore, it is highly desirable to adopt wear-resistant tool materials to avoid tool wear, with polycrystalline cubic boron nitride (PCBN) being a good choice [33]. Furthermore, surface hardening coating of a steel tool might be an alternate approach to increase wear resistance [9].

## 5. Conclusions

1. FSW resulted in the generation of the fine and equiaxed recrystallized grains and the breaking and uniform distribution of the SiC particles in the nugget zone. Post-weld T4-treatment did not result in significant grain growth.
2. The onion rings, observed in the nugget zone of the FSW composite, consisted of fine particle-rich bands, and were devoid of the SiC particle segregation.
3. The tensile and yield strengths of the as-FSW composite welds in both longitudinal and transverse directions were superior to those of the as-extruded base metal.
4. Under the T4 condition, the tensile strength of the welds along the longitudinal and transverse directions reached 82% and 95% of the base metal, respectively. Formation of the $Cu_2FeAl_7$ phase was responsible for the lower strength of FSW joints compared to base materials under the T4 condition.

## Acknowledgments

The authors gratefully acknowledge the support of (a) the National Outstanding Young Scientist Foundation for Z.Y. Ma under Grant No. 50525103, and (b) the Hundred Talents Program of Chinese Academy of Sciences.

## References

[1] Storjohann D, Barabash OM, Babu SS, David SA, Sklad PS, Bloom EE. Fusion and friction stir welding of aluminum–metal–matrix composites. Metall Mater Trans 2005;A36:3237–47.
[2] Mishra RS, Ma ZY. Friction stir welding and processing. Mater Sci Eng 2005;R50:1–78.
[3] Thomas WM, Nicholas ED, Needham JC, Murch MG, Templesmith P, Dawes CJ, G B Patent Application No.9125978.8; December 1991.
[4] Nelson TW, Zhang H, Haynes T. Friction stir welding of aluminum MMC 6061-Boron carbide. In: Proc. 2nd Int Symposium on Friction Stir Welding, Gothenburg, Sweden; 2000.

[5] Mahoney MW, Harrigan WH, Wert JA. Friction stir welding SiC discontinuously reinforced aluminum. INALCO'98, Cambridge, UK, vol. 2; 1998. p. 231–6.
[6] Cavaliere P, Cerri E, Marzoli L, Santos JD. Friction stir welding of ceramic particle reinforced aluminum based metal matrix composites. Appl Compos Mater 2004;2:247–58.
[7] Marzoli LM, Strombeck AV, Santos JFD, Gambaro C, Volpone LM. Friction stir welding of an AA6061/Al2O3/20p reinforced alloy. Compos Sci Technol 2006;66:363–71.
[8] Nakata K, Inoki S, Nagano Y, Ushio M. Friction stir welding of Al2O3 particulate 6061 Al alloy composite. Mater Sci Forum 2003;426–432:2873–8.
[9] Uzun H. Friction stir welding of SiC particulate reinforced AA2124 aluminum alloy matrix composite. Mater Des 2007;28:1440–6.
[10] Cavaliere P. Mechanical properties of friction stir processed 2618/Al2O3/20p metal matrix composite. Compos Part A – Appl S 2005;36:1657–65.
[11] Ceschini L, Boromei I, Minak G, Morri A, Tarterini F. Effect of friction stir welding on microstructure, tensile and fatigue properties of the AA7005/10 vol.% $Al_2O_3$p composite. Compos Sci Technol 2007;67:605–15.
[12] Humphreys FJ. A unified theory of recovery, recrystallization and grain growth, based on the stability and growth of cellular microstructures-2. The effect of second-phase particles. Acta Mater 1997;45:5031–9.
[13] Hassan KAA, Norman AF, Price DA, Prangnell PB. Stability of nugget zone grain structures in high strength Al-alloy friction stir welds during solution treatment. Acta Mater 2003;51:1923–36.
[14] Ma ZY, Feng AH, Xiao BL, Fan JZ, Shi LK. Microstructural evolution and performance of friction stir welded aluminum matrix composites reinforced by SiC particles. Mater Sci Forum 2007;539–543:3814–9.
[15] Feng AH, Ma ZY. Formation of $Cu_2FeAl_7$ phase in friction stir welded SiCp/Al–Cu–Mg composite. Scripta Mater 2007;57:1113–6.
[16] Krishnan KN. On the formation of onion rings in friction stir welds. Mater Sci Eng 2002;A327:246–51.
[17] Schneider JA, Nunes AC. Characterization of plastic flow and resulting microtextures in a friction stir weld. Metall Mater Trans 2004;B35:777–83.
[18] Sutton MA, Yang B, Reynolds AP, Taylor R. Microstructural studies of friction sir welds in 2024-T3 aluminum. Mater Sci Eng 2002;A323:160–6.
[19] Hatch JE. Aluminum properties and physical metallurgy. Metals Park, Ohio: American Society for Metals; 1984. p. 121.
[20] Su JQ, Nelson TW, Mishra RS, Mahoney M. Microstructural investigation of friction stir welded 7050-T651 aluminum. Acta Mater 2009;51:713–29.
[21] Su JQ, Nelson TW, Sterling CJ. Microstructure evolution during FSW/FSP of high strength aluminum alloys. Mater Sci Eng 2005;A405:277–86.
[22] Montheillet F, Lepinoux J, Weygand D, Rauch E. Dynamic and static recrystallization. Adv Eng Mater 2001;3:587–9.
[23] Xia XX, Mcqueen HJ. Deformation behaviour and microstructure of a 20% $Al_2O_3$ reinforced 6061 Al composite. Appl Compos Mater 1997;4:333–47.
[24] Ko BC, Yoo YC. Prediction of dynamic recrystallization condition by deformation efficiency for Al 2024 composite reinforced with SiC particle. J Mater Sci 2000;35:4073–7.
[25] Inem B. Dynamic recrystallization in a thermomechanically processed metal matrix composite. Mater Sci Eng 1995;A197:91–5.
[26] Humphreys FJ, Hatherly M. Recrystallization and related annealing phenomena. Pergamon; 1996. p. 269.
[27] Humphreys FJ, Miller WS, Djazeb MR. Microstructural development during thermomechanical processing of particulate metal–matrix composites. Mater Sci Technol 1990;6:1157–66.
[28] Chang CI, Lee CJ, Huang JC. Relationship between grain size and Zener–Holloman parameter during friction stir processing in AZ31 Mg alloys. Scripta Mater 2004;51:509–14.
[29] Heurtier P, Desrayaud C, Montheillet F. A thermomechanical analysis of the friction stir welding process. Mater Sci Forum 2002;396–402:1537–42.
[30] Klug HP, Alexander LE. X-ray diffraction procedures for polycrystalline and amorphous materials. 2nd ed. New York: John Wiley & Sons; 1974. p. 549.
[31] Villars P, Prince A, Okamoto H. Handbook of ternary alloys phase diagrams [M], ASM International, OH44073, USA, The Materials Society, CDROM; 1997.
[32] Genevois C, Deschamps A, Denquin A, Cottignies BD. Quantitative investigation of precipitation and mechanical behavior for AA2024 friction stir welds. Acta Mater 2005;53:2447–58.
[33] Sorensen CD, Nelson TW. Tool material testing for FSW of high-temperature alloys. In: Packer S, editor, 3rd Int Symposium on Friction Stir Welding, Kobe, Japan; September 2001.